Ultrasound characterization of red blood cells distribution: a wave scattering simulation study

Emilie Franceschini, Bruno Lombard, Joël Piraux

Laboratoire de Mécanique et d'Acoustique LMA - CNRS UPR 7051, 13402 Marseille cedex 20, France

E-mail: franceschini@lma.cnrs-mrs.fr

Abstract. Ultrasonic backscattered signals from blood contain frequency-dependent information that can be used to obtain quantitative parameters describing the aggregation state of red blood cells (RBCs). However the relation between the parameters describing the aggregation level and the backscatterer coefficient needs to be better clarified. For that purpose, numerical wave simulations were performed to generate backscattered signals that mimic the response of two-dimensional (2D) RBC distributions to an ultrasound excitation. The simulated signals were computed with a time-domain method that has the advantages of requiring no physical approximations (within the framework of linear acoustics) and of limiting the numerical artefacts induced by the discretization of object interfaces. In the simple case of disaggregated RBCs, the relationship between the backscatter amplitude and scatterer concentration was studied. Backscatter coefficients (BSC) in the frequency range 10 to 20 MHz were calculated for weak scattering infinite cylinders (radius 2.8 μm) at concentrations ranging from 6 to 36%. At low concentration, the BSC increased with scatterer concentrations; at higher concentrations, the BSC reached a maximum and then decreased with increasing concentration, as it was noted by previous authors in *in vitro* blood experiments. In the case of aggregated RBCs, the relationship between the backscatter frequency dependence and level of aggregation at a concentration of 24% was studied for a larger frequency band (10 - 50 MHz). All these results were compared with a weak scattering model based on the analytical computing of the structure factor.

1. Introduction

The aggregation of red blood cells (RBCs) is a physiological reversible process. When RBCs are under low shear rates ($<$10 s^{-1}), they interact strongly with each other and form complex 3D rouleaux structures. When the shear rate increases, rouleaux structures desaggregate. This phenomenon is not pathological. However, RBC hyper-aggregation, an abnormal increase of RBCs aggregation, is a pathological state associated with several circulatory diseases such as deep venous thrombosis, atherosclerosis and diabetes mellitus. These pathologies inflict particular sites (inferior members for thrombosis, arterial bifurcations for atherosclerosis, the foot and eye for diabetes). Ultrasonic imaging holds the perspective of further elucidating the role of RBC aggregation on the etiology of these diseases *in vivo* and *in situ*.

Classical blood characterization techniques consist of measuring the magnitude and frequency dependence of the radio frequency backscatter spectrum. A large number of *in vitro* experiments on blood have been performed to study how these two indices vary with shear rate, flow turbulence, hematocrit (i.e. concentration of RBCs), and RBC aggregation level [1]-[4].

Theoretical efforts have been also made to develop ultrasound backscattering models for non-aggregating [5] and aggregating RBCs [6]. Twersky [5] proposed a packing factor to describe the backscattering coefficient of a distribution of hard particles. This model succeeds to explain the relationship between the backscatter amplitude and hematocrit for non-aggregating RBCs but fails to predict the frequency dependence observed in *in vitro* experiments when considering aggregating RBCs. Yu and Cloutier [6] recently parametrized the backscattering coefficient from blood: two indices describing RBC aggregation, the packing factor and mean aggregate diameter, were extracted from the Structure Factor Size Estimator. However this estimator still needs to be quantitavely evaluated.

The purpose of this paper is to perform numerical ultrasound wave simulations through 2D RBC distributions in order to validate a weak scattering theoretical model based on a particle approach [7]. This theoretical model is commonly employed for approximating the ultrasound backscattering from RBCs [8]-[12]. In order to simulate ultrasonic propagation through RBCs, we use a time-domain numerical method [13] [14] that has the advantages of requiring no physical approximation (within the framework of linear acoustics) and of limiting the numerical artefacts induced by the discretization of object interfaces. Our method therefore automatically accounts for multiple scattering, refraction, and reflection, and the accuracy of the numerical solution is independent of the cell number. In the simple case of disaggregated RBCs, the relationship between the backscatter amplitude and scatterer concentration is studied. In the aggregating case, the relationship between the backscatter frequency dependence and level of aggregation at a concentration of 24% is studied in the frequency range 10 to 50 MHz. All the results obtained from the direct numerical simulation are compared with those expected from theory.

2. Ultrasound backscattering theory

Ultrasonic scattering from blood is mainly caused by the RBCs. Indeed, blood can be mechanically described as a colloidal suspension of RBCs in plasma. RBCs constitute the vast majority (97%) of the cellular content of blood and occupy a large volume fraction (hematocrit) of 35-45% under normal conditions. In this 2D study, RBCs are modeled as parallel infinite cylinders of radius a, that have a small acoustical impedance contrast relatively to the host homogeneous medium (i.e. the plasma): $\gamma_z = (Z_{RBC} - Z_{plasma})/Z_{plasma}$. RBCs and plasma are assumed to be fluid and non-dissipative media. In the following, we recall the scattering model commonly used for a single RBC and then for many RBCs.

2.1. Single-RBC scattering model

Consider a backscattering configuration that consists of the insonification of one fluid RBC by a monochromatic plane wave $p_i(\mathbf{r}) = p_0 e^{i\mathbf{kr}}$, where $\mathbf{r}$ is the spatial vector, p_0 is the incident pressure amplitude, and $\mathbf{k}$ represents the wave vector ($|\mathbf{k}| = k = 2\pi/\lambda$, λ being the wavelength). In the far field of the particle, the field backscattered by the particle has the asymptotic form:

$$p_s(\mathbf{r}) = p_0 \frac{e^{i\mathbf{kr}}}{\sqrt{r}} \left[\sigma_b(k)\right]^{1/2}, \tag{1}$$

where σ_b is the backscattering cross section per unit area of one particle that can be calculated using the theory of Faran [15]. For the simplest case where the particle size is small compared to wavelength ($ka << 1$), we use Rayleigh scatterer form [16]

$$\sigma_b(k) = \frac{1}{2\pi^2} k^3 A_p^2 \gamma_z^2 \left(\frac{J_1(2ka)}{ka}\right)^2, \tag{2}$$

where $A_p = \pi a^2$ is the particle area and J_1 is the first order Bessel function of the first kind.

2.2. Many-RBC scattering model

The theoretical model of ultrasound backscattering by blood is based on a particle approach[6] [7], which consists of summing contributions from individual RBCs and modeling the RBC interaction by a structure factor. By using the Born approximation (weak scattering) and considering a collection of n identical and cylindrical RBCs in the backscattering configuration described in the previous section, the differential backscattering cross section per unit area (also called the backscattering coefficient BSC) can be written as [5]:

$$BSC_{theo}(k) = m\sigma_b(k)S(k), \tag{3}$$

where m is the number density of RBCs in blood that is related with the hematocrit H as $m = H/A_p$. The function S is the structure factor representing the spatial positioning of particles and defined by:

$$S(\mathbf{k}) = E\left[\frac{1}{n}\left|\sum_{i=1}^{n} e^{-i2\mathbf{k}\mathbf{r}_i}\right|^2\right] \tag{4}$$

where E represents the expected value of a random variable and $\mathbf{r}_i$ the position vectors defining the center of the ith scatterer in space. Since the medium is isotropic, $S(\mathbf{k})$ depends only on k; for the clarity of the notation, we confused $S(\mathbf{k})$ and $S(k)$ as done in Eq. (3). The aggregation phenomenon is thus supposed to only affect the structure factor since RBCs properties and hematocrit remain constant in the region of interest.

In the low frequency limit, the structure factor tends towards a constant value $S(k) \to S(0) = W$ called the packing factor that has been extensively studied for non-aggregating particles. The most often used packing factor expression is based on the Percus-Yevick pair-correlation function for identical, hard and radially symmetric particles. The Perkus-Yevick packing factor W_{PY} was first applied to blood by Shung [17] and is related in the 2D space with the hematocrit as [5] [17] [7]

$$W_{PY} = \frac{(1-H)^3}{1+H}. \tag{5}$$

At very low H, W_{PY} is equal to unity. As H increases, W_{PY} decays to zero so that the BSC also approaches zero at very high H because in a densely packed medium one can always find an RBC that will destructively interfere with the contribution from another RBC.

3. Methods

3.1. Computation of a RBCs distribution

We describe here how random distributions for non-aggregating and aggregating RBCs were computed. These distributions were employed in the direct numerical simulation and in the computation of the theoretical BSC.

Computation of a random distribution for non-aggregating RBCs. First, we specify the RBC radius $a = 2.75\mu$m and the surface size S to be investigated. For each studied hematocrit H, the number of RBCs n is given by $n = HS/A_p$ and then a simple method allows the determination of the RBC spatial positions as described in the following. The center position of each cylinder is determined by a pair of random variables (x_i, y_j). Each time a new cylinder is placed, a procedure is applied to check the distance between the newly generated cylinder and the cylinders generated before. If a newly generated scatterer overlaps with any other scatterers, the scatterer will be discarded, otherwise the scatterer's position is saved. This procedure is repeated until the required hematocrit is reached. Note that, for each hematocrit, two types of distribution were performed:

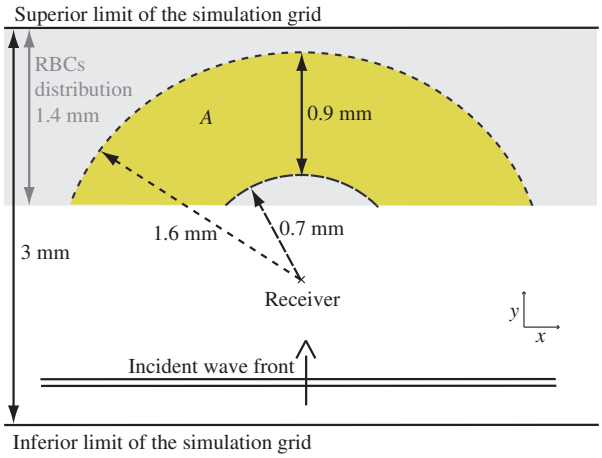

Figure 1. Sketch of the computational domain. The area of interest A is the zone containing the RBCs distribution and located between the two arcs of circles. The center of these circles corresponds to the receiver position and the circle radii are 0.7 mm and 1.6 mm.

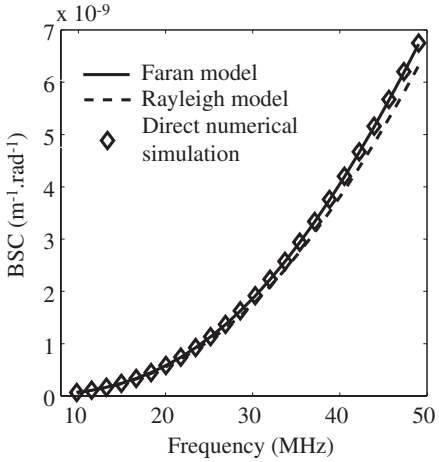

Figure 2. Backscattering cross sections per unit area σ_b of a single RBC. The solid and dashed lines display σ_b given by, respectively, the Faran and Rayleigh models. Simulations results are shown by the symbols.

- one with an exclusion length l_e=0.9μm between scatterer (i.e. a non-zero minimal length between scatterer interfaces) for computational purpose in the direct numerical simulation (see section 3.2),
- one without an exclusion length, i.e. scatterers could be in contact.

Computation of a random distribution for aggregating RBCs. First, discs of radius 6.60 μm (and respectively 9.08 μm) are randomly generated, these discs correspond to aggregates containing 3 RBCs (and respectively 6 RBCs). An exclusion length l_e is ensured between aggregates. For a specific hematocrit, the locations of the scatterers inside each aggregate are generated randomly with an exclusion length l_e between scatterers.

3.2. Direct numerical simulation

The numerical method used to compute the solution of the wave equation was previously described [13] [14]. The time-domain numerical integration of acoustic equations is done by a second-order Lax-Wendroff scheme. The discretization of interfaces is done by an immersed interface method, ensuring accurate description of geometrical features and of the jump conditions. The computations involve grids of 2 mm×3 mm with mesh sizes $\Delta x = \Delta y = 0.195$ μm (i.e. grids of 10240×15360 nodes) requiring the parallelization of algorithms on a cluster of PCs. The RBCs are distributed on a 2 mm × 1.4 mm rectangular subdomain. As required by the immersed interface method, an exclusion length l_e between each scatterer is taken equal to $4\Delta x$=0.9 μm.

The computational grid is excited by a plane wave whose support is originally outside the region of interest. The x axis of the computational domain are periodized in order to simulate the wave propagation in a semi-infinite medium (see Fig. 1). At each time step, the simulated acoustic pressure is recorded on 256 receivers. These receivers are placed at every 8 μm and in parallel to the incident wave front in order to simulate a transducer moved laterally. Signals

were selected with a rectangular window of length 0.9 mm centered at a distance $d = 1.15$ mm from the receivers. The power spectra of the 256 backscattered signals were then averaged to provide the mean backscattered power spectrum $\overline{P}$. The BSC obtained from the simulated data was computed as

$$BSC_{sim}(k) = \frac{d}{A}\frac{\overline{P}}{P_{inc}}, \tag{6}$$

where P_{inc} is the power spectrum of the incident signal and A is the area of interest determined by acoustic ray theory. Indeed, since signals are selected with a rectangular window corresponding to depths between 0.7 mm and 1.6 mm from the receivers, the RBCs contributing to the selected signals are localized between two circles of radii 0.7 mm and 1.6 mm and of center the receiver positions. The area of interest A is thus the zone containing the RBCs distribution and located between these two circles as shown in Fig. 1.

3.3. Computation of the theoretical BSC

The computation of the theoretical BSC requires the knowledge of the structure factor as described in Eq. (3). Since S is by definition a statistical quantity, an average of all structure factors obtained from several random particle distributions can give an estimated value of S. For each particle distribution, a matrix D was computed by dividing the square simulation plane L^2 in N_p^2 pixels and by counting the number of particles falling into each pixel, N_p being sufficiently high in order that there is a maximum of one particle by pixel. We chose to take L=300 μm and N_p=256 pixels as a tradeoff between the computational domain size and the computational time. This matrix D represents the microscopic density function defined by $D(\mathbf{r}) = \sum_{i=1}^{n} \delta(\mathbf{r} - \mathbf{r}_i)$, where δ is the Dirac distribution. According to Eq.(4), the structure factor can thus be described by:

$$S(\mathbf{k}) = E\left[\frac{1}{n}\left|\int D(\mathbf{r})e^{-i2\mathbf{kr}}d\mathbf{r}\right|^2\right]. \tag{7}$$

The structure factor was thus computed by averaging 2-D fast Fourier transforms (2D FFT) of 200 density matrix D. This FFT gave the structure factor values $S(\mathbf{k})$ on a centered grid of wavevectors between $\pm\pi N_p/2L$ with a step of $\Delta k = \pi/L$. The theoretical BSC is then obtained using Eq. (3).

4. Results and discussion

4.1. Non-aggregating case

Figure 2 shows the simulated σ_b as a function of frequency in a linear scale. Also represented are two theoretical σ_b obtained from the Rayleigh and Faran models. One can notice that the Faran model matches well the σ_b obtained with the direct numerical simulation at all frequencies, whereas the Rayleigh model is only valid within 5% accuracy until a frequency of 22 MHz. Note that this result was expected since the Rayleigh model is accurate within 5% for ka <0.25. In the following, all the theoretical BSCs presented will be calculated using the Faran model.

For non-aggregating RBCs at low frequencies, the relationship between the BSC amplitude and hematocrit was investigated. Figure 3a presents four averaged BSCs obtained by averaging BSCs between frequencies in the validity domain of Rayleigh behavior (i.e. between 10 and 22 MHz). The diamond markers represent the simulation results. The solid line shows the prediction by the hard sphere Percus-Yevick packing factor. The dashed lines indicate the particle theory approach by considering RBC distributions with and without an exclusion length.

This figure demonstrates that both simulation results and particle theory approach with the same exclusion length are in good agreement at low frequencies. For the results without an

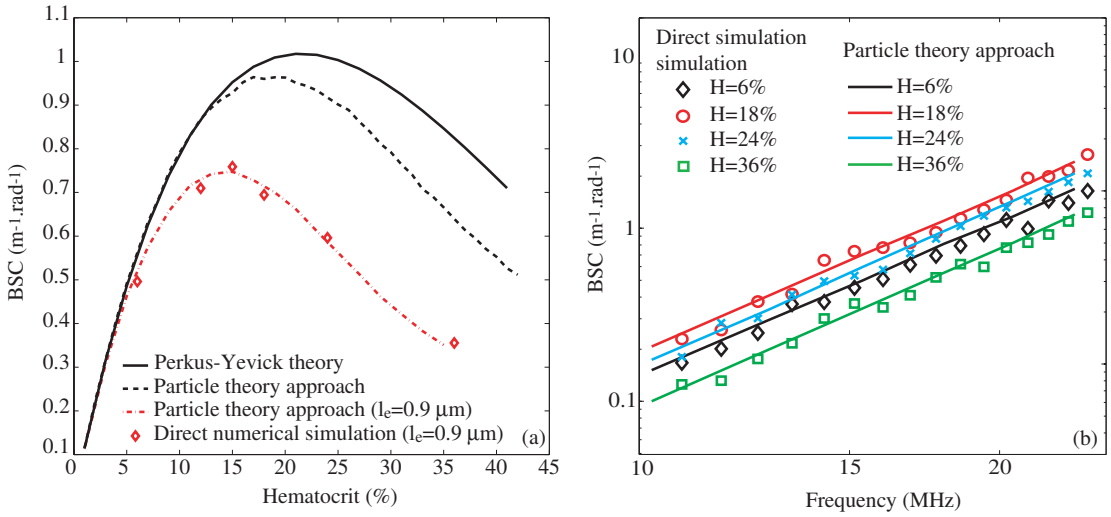

Figure 3. (a) Plots of backscatter coefficients versus the hematocrit for non-aggregated RBCs. The solid curve represents the BSC_{theo} calculated with the Percus-Yevick packing factor, the dashed lines the particle theory approach BSC_{theo} obtained by computing the structure factor with and without the exclusion length. The diamond markers express simulation results BSC_{sim}. (b) Frequency-dependent backscattering coefficients for an hematocrit of 6, 18, 24 and 36% in the case of non-aggregated RBCs. The solid line represents the curve for the particle theory approach. Simulations results are shown by the symbols.

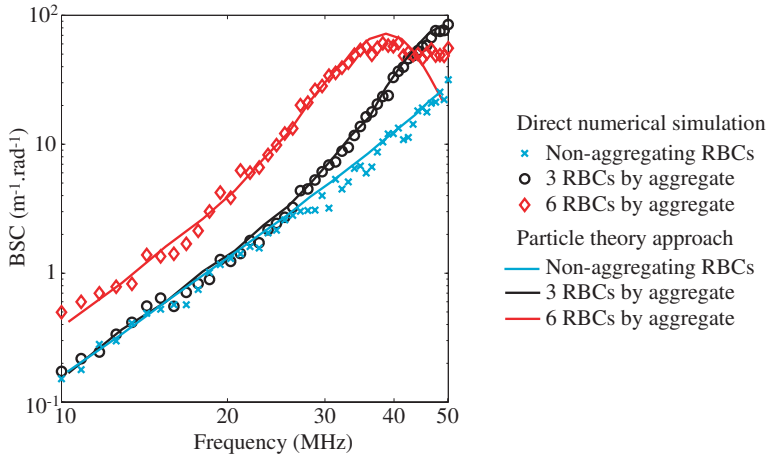

Figure 4. Frequency-dependent backscattering coefficients for a constant hematocrit of 24 % in the case of non-aggregated and aggregated RBCs. The solid line represents the curve for the particle theory approach. Simulations results are shown by the symbols.

exclusion length, the peak of the BSC obtained by the particle theory approach is seen at about 19%, in close agreement with the Percus-Yevick packing theory at about 22% as observed by Zhang and co-workers [8] with a Gaussian pulse incident wave (see Fig. 10 in Ref. 19). However, from a quantitative point of view, the Percus-Yevick packing theory does not match the particle theory approach for hematocrits superior to 14 %.

Typical results of the frequency-dependent BSC_{sim} and BSC_{theo} for an hematocrit of 6, 18, 24 and 36% are given in Fig. 3b in a log compressed scale. For both BSCs, the distributions

were realized with the exclusion length l_e. Standard deviations are not shown for clarity. The weak scattering model based on the structure factor matches quite well the simulation results. For all hematocrits, the BSCs are Rayleigh at low frequencies (up to 22 MHz) i.e. the BSCs have third-power frequency dependence.

To conclude the non-aggregation case study, for the RBC distributions having an exclusion length, the direct numerical simulation validates the structure factor theory for frequencies between 10 and 22 MHz. We can reasonably extrapolate this result to RBC distributions without an exclusion length. As shown in Fig. 3a, it will be thus more accurate to calculate the theoretical BSC via the particle theory approach rather than the Percus-Yevick packing theory for dense medium.

4.2. Aggregating case

Figure 4 shows the simulated and theoretical BSCs as a function of frequency in a log compressed scale in the case of aggregating RBCs. A constant hematocrit H=24% and two aggregate sizes (i.e. 3 and 6 RBCs by aggregate) were used for these computations. The markers represent the simulation results and the solid line shows the prediction by the particle theory approach. As observed in the case of the non-aggregating case in Fig. 3b, the particle theory approach matches quite well the simulation results. However, for the largest level of aggregation and for high frequencies (>40 MHz), the structure factory model fails to simulate the backscattered field.

Also represented in Fig. 4 are the results in the case of non-aggregated RBCs at an hematocrit of H=24% in order to compare non-aggregating and aggregating cases. For non-aggregated RBCs, the slope of the BSC as a function of frequency is linear in our log-log scale. When considering aggregated RBCs, the BSC becomes non-Rayleigh: the slope becomes not linear in our log-log scale and the BSC amplitude increases as the level of aggregation becomes larger. Note that the behaviors (frequency-dependence and amplitude) of the BSC in both non-aggregated and aggregated RBCs were the same in *in vitro* experiments performed by Yu and Cloutier [6] in a controlled Couette flow.

5. Conclusion

This study shows that the particle theory approach approximates accurately the backscattering field of ultrasonic waves when the wavelength of the incident field is much greater than the scatterer size, for hematocrits inferior to 36% and for frequencies between 10 and 40 MHz. Future works will incorporate elastic waves in the direct numerical simulation.

[1] Yuan W and Shung K K 1988 *J.Acoust. Soc. Am.* **84**, 1195-1200
[2] Foster F S, Obara H, Bloomfield T, Ryan L K and Lockwood G R 1994 *IEEE Ultrasonics Symposium Proceedings* 1599-1602
[3] Van Der Heiden M S, De Kroon M G, Bom N and Borst C 1995 *Ultrasound Med. Biol.* **21** 817-26
[4] Cloutier G, Qin Z, Durand L G and Teh B G 1996 *IEEE Trans. Biomed. Eng.* **43** 441-50
[5] Twersky V 1987 *J. Acoust. Soc. Am.* **81** 1609-18
[6] Yu F T H and Cloutier G 2007 *J. Acoust. Soc. Am.* **122**, 645-56
[7] Mo L Y L and Cobbold R S C 1993 *Ultrasonic Scattering in Biological Tissues* (CRC, Boca Raton, FL) chapter 5 pp 125-170
[8] Zhang J, Rose J L and Shung K K 1994 *Ultrasound in Med. Biol.***20** 903-913
[9] Fontaine I, Bertrand M and Cloutier G 1999 *Biophysical Journal* **77** 2387-99
[10] Savery D and Cloutier G 2005 *IEEE Trans. Ultrason. Ferroelectr. Freq. Control* **52** 94-103
[11] Franceschini E, Yu F T H, Fenech M and Cloutier G 2007 *IEEE Ultrasonics Symposium Proceedings* 2503-06
[12] Saha R K and Cloutier G *Physical review* E**78** 061919
[13] Piraux J and Lombard B 2001 *Journal of Computational Physics* **168** 227-48
[14] Lombard B and Piraux J 2004 *Journal of Computational Physics* **195** 90-116
[15] Faran J J 1951 *J. Acoust. Soc. Am.* **23** 405-418

[16] Insana M F and Brown D G 1993 *Ultrasonic Scattering in Biological Tissues* (CRC, Boca Raton, FL) chapter 5 pp 75-124
[17] Shung K K 1982 *IEEE Trans. Ultras., Ferroelect., Freq. Contr.* **SU-26**, 327-31